2mic4

**NASA TECHNICAL MEMORANDUM**

NASA TM X-71495

NASA TM X-71495



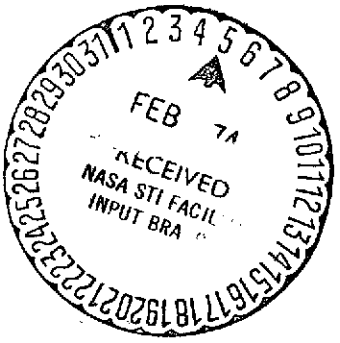


# EFFECT OF CONFIGURATION VARIATION ON EXTERNALLY BLOWN FLAP NOISE

by Robert G. Dorsch, Jack H. Goodykoontz,
and Noel B. Sargent
Lewis Research Center
Cleveland, Ohio

TECHNICAL PAPER proposed for presentation at
Twelfth Aerospace Sciences Meeting sponsored by
the American Institute of Aeronautics and Astronautics
Washington, D.C., January 30 - February 1, 1974

# EFFECT OF CONFIGURATION VARIATION ON EXTERNALLY BLOWN FLAP NOISE

R. G. Dorsch,* J. H. Goodykoontz,* and N. B. Sargent*
Lewis Research Center
National Aeronautics and Space Administration
Cleveland, Ohio 44135

## Abstract

The sensitivity of flap interaction noise to variations in engine-under-the-wing externally blown flap geometry was investigated with a large cold-flow model. Both 2- and 3-flap wing sections (7-ft chord) with trailing flap angles up to 60° were employed. Exhaust nozzles included coaxial, plug, and 8- and 13-inch diameter conical configurations. These nozzles were tested at two positions below the wing ($19\frac{1}{4}$ and $29\frac{1}{4}$ in.). The effects of these geometry variations on noise level, directivity, and spectral shape are summarized in terms of exhaust flow parameters evaluated at the nozzle exit and at the flap impingement station. The results are also compared with limited flap noise data available from tests using real engines.

E-7858

## Introduction

The use of externally blown flaps (EBF) to achieve powered lift for short haul aircraft applications is currently under consideration. Both engine-under-the-wing and engine-over-the-wing configurations are being examined. Unfortunately a considerable amount of noise is produced as the engine exhaust flows over either the upper or lower surfaces of the wing-flap system.(1-10)

This paper will examine the sensitivity of the flap noise produced by a cold-flow model of the engine under-the-wing EBF system to changes in configuration geometry. Configuration variations were achieved by making simple alterations to the basic EBF model of reference 3. Parameters varied were nozzle type and size, number of flaps, nozzle location below the wing, flap deflection angles, and wing sweepback angle. Nozzle types tested included a coaxial, an annular nozzle with a conical centerbody (plug nozzle), and 8- and 13-inch-diameter conical nozzles. Both 2- and 3-flap EBF configurations were tested at trailing flap angles up to 60°.

The flap noise data obtained in these tests will be summarized in terms of the effect of configuration changes on noise radiation patterns, spectral shape, and sound pressure level. The flap noise data are compared using two different sets of exhaust flow parameters. One set of parameters was measured at the nozzle exit plane and the other set was

*Aerospace Research Engineers, V/STOL and Noise Division.

measured at the flap impingement station. The results are also compared with limited flap noise data available from tests using real engines.

## Symbols

$A$ area of exhaust jet normal to nozzle centerline, $ft^2$

$A_C$ area of core nozzle exit, $ft^2$

$A_F$ area of annular fan nozzle exit, $ft^2$

$A_i$ impingement area based on $d_i$, $ft^2$

$A_N$ area of conical nozzle exit, $ft^2$

$A_T$ nozzle exit total area ($A_C + A_F$ for coaxial nozzle), $ft^2$

$C_O$ ambient speed of sound, ft/sec

$D$ nozzle exit diameter, ft

$D_C$ core nozzle exit diameter, ft

$D_T$ equivalent diameter of nozzle based on total exit area $A_T$, ft

$d_i$ diameter of radial impingement velocity profile where velocity has dropped to 80 percent of peak value, ft

$\Delta f$ band-width of 1/3-octave filter, Hz

$I_i$ turbulent intensity; from turbulent intensity profile measured at X without presence of wing, dimensionless

$M_C$ Mach number of nozzle core exhaust, dimensionless

$M_N$ Mach number of conical nozzle exhaust, dimensionless

$R$ microphone circle radius, ft

$p$ RMS acoustic pressure, microbars

$V$ exhaust velocity, ft/sec

$V_C$ core nozzle exhaust velocity, ft/sec

$V_E$ effective nozzle exhaust velocity, ft/sec

$V_F$ fan (annulus) nozzle exhaust velocity, ft/sec

$V_i$ impingement velocity; from velocity profile measured at X without presence of wing, ft/sec

$V_{i,p}$ peak impingement velocity, ft/sec

$V_N$ conical nozzle exhaust velocity, ft/sec

X impingement distance; distance along nozzle centerline from exhaust plane to point of intersection with flap assembly, ft

Y distance from nozzle centerline axis to wing chordline, in.

$\theta$ microphone radial angle measured from nozzle inlet direction, deg

$\rho_o$ ambient density, slugs/ft$^3$

## Apparatus and Procedure

### Model Configurations

Baseline models. The baseline EBF configurations are shown in Figures 1 to 3. The 2-flap configurations shown in Figure 1 are identical to those previously described in Reference 3. The geometry of the three-flap versions of the basic EBF model is shown in Figures 2 and 3. The configurations shown in Figure 2 have the same 13-inch-diameter conical nozzle (circular convergent) as Figure 1(b) and the configurations of Figure 3 have the same coaxial nozzle as Figure 1(a). The core nozzle of the coaxial assembly was circular with an 8.15-inch diameter and the annular nozzle (fan exhaust) had an inner diameter of 18 inches and an outer diameter of 23.25 inches. The annulus height was 2.63 inches. The baseline exhaust nozzles of Figures 1 to 3 were all located so that the nozzle centerline was 19.25 inches below the wing chordline. The conical nozzle (Figs. 1(b) and 2) was positioned so that the exhaust plane was 15 inches ahead of the wing leading edge. The coaxial nozzle was positioned with the annular exit 15 inches ahead and the core exhaust plane 7 inches downstream of the wing leading edge (Figs. 1(a) and 3). The wing section of the basic model had a nominal chord length of 82 inches (with the flaps retracted).

The EBF model was mounted with the 9-foot-span wing section in a vertical position with the axis of the nozzle located 12.75 feet above grade. The nozzle centerline (axis) was located at a spanwise position 5 feet from the bottom of the wing section and 4 feet from the top to minimize support structure interference with spanwise flow on the flaps. Photographs of the baseline 3-flap model are shown in figure 4. Figure 4(a) shows the model in the configuration of Figure 2(b) and Figure 4(b) shows the model of Figure 3(b). The baseline wing model was unswept.

Variations. Several models having simple variations to the baseline geometries of Figures 1 to 3 were tested. These configurations are included in Table 1 along with key geometric variables.

The simplest variation tested was the 3-flap model (Figs. 2 and 3) with the nozzle centerline axis to wing chordline distance (Y) increased by 10 inches. This placed the nozzle centerline 29.25 inches below the wing chordline. The models were designed so that although the nozzle centerline intersected the flap assembly at a lower point, the impingement distance (X of Figs. 2 and 3) did not change for the $60^{\circ}$ trailing flap configurations. The impingement distance did change for the $20^{\circ}$ trailing flap models. Values of X and Y are given for each configuration in Table 1 along with flap angle settings.

By simple conversions of the coaxial nozzle assembly, the 2-flap configuration of Figure 1(a) was tested with an 8.15-inch-diameter conical nozzle and with a plug nozzle. The annulus was blocked off by an internal bell mouth assembly to convert the coaxial nozzle to an 8.15-inch-diameter conical nozzle. The plug nozzle was obtained by blocking the core nozzle of the coaxial assembly with a 12.75 inch long $33^{\circ}$ cone (blunt tip). The cone acted as a centerbody for the annular flow from the 23.25-inch-diameter annulus.

The effect of wing sweep-back on the flap noise was determined by running one test with baseline configuration 1(b) with the wing section at a $16^{\circ}$ sweep angle instead of in the usual unswept position. A photograph of the swept wing model is shown in Figure 5. In order to maintain X = 72 inches, the 13-inch conical nozzle was mounted approximately 13 inches ahead of the wing leading edge at the nozzle axis; otherwise the geometry was the same as in Figure 1(b).

## Air Flow System

The exhaust nozzles were supplied with ambient dry air from the Center's propulsion air supply system (150 psig max.) brought to the test site by a 24-inch diameter underground line. An orifice flowmeter was located in a straight section of the underground line upstream of a 16-inch gate shutoff valve at the test site. The EBF test rig flow system shown in Figure 6 was connected to the gate valve. The test rig had two flow distribution and quieting screens located between the last elbow of the flow system and the nozzle assemblies.

The operating pressure ratio (nozzle total pressure divided by the ambient atmospheric pressure) for the coaxial nozzle core and the 13-inch convergent nozzle was set by the flow control valve and supply pressure. A pressure drop screen in the annulus of the coaxial nozzle assembly determined the corresponding pressure ratio for the simulated fan exhaust. The screen provided a nominal ratio of fan exhaust velocity to core exhaust velocity of 0.78. This ratio varied from about 0.65 at a core PR of 1.1 to 0.83 at a PR of 1.8.

Nozzle total pressures and temperatures were measured at the nozzle inlets (downstream of the screen in the case of the annular nozzle). The nozzle exhaust velocities were determined from the fully expanded isentropic equations.

Internal Noise Suppression

The muffler system (Fig. 6) consisted of overlapping low, middle, and high frequency attenuators. Low frequency quieting was obtained by the use of perforated plates as pressure drop devices just downstream of the flow control valve (the principal noise source) and at the exit of the middle frequency muffler. These plates have a low admittance to low frequency noise and also serve as flow redistributors.

The middle frequency muffler consisted of a 3-foot diameter 6-foot long pipe with crossed splitter plates to divide the flow into four channels. All inside surfaces were lined with 1-inch thick hair felt held in place by expanded metal (70 percent open). The perforated plate at the end of this section had 1/8-inch diameter holes and was 20 percent open.

The high frequency muffler section was located at the downstream end of the upper (and last) elbow of the flow system to take advantage of multiple reflections associated with the flow turn. A crossed splitter plate divided the flow into four channels. All inside pipe walls and both sides of the horizontal splitter plate were lined with one-inch thick plastic felt material held in place by expanded metal (70 percent open). The first of the final two flow distribution and quieting screens was located immediately downstream of this muffler.

Finally, to prevent direct radiation of internal noise transmitted through the pipe walls the flow system was wrapped with a 2-inch thick layer of fiberglass covered by leaded-vinyl plastic sheet material.

Acoustic Instrumentation and Analysis

The noise data were measured with twenty 1/2-inch condenser microphones located 12.75 feet above a hard surface (black top). The microphones were placed on a 50-foot radius circle in a horizontal plane perpendicular to the vertically mounted wing. The center of the microphone circle was located on the nozzle-axis centerline halfway between the core nozzle exhaust exit plane and the point of intersection with the $60^{\circ}$ flap (Fig. 1(a)).

The noise data were analyzed on-line with an automated 1/3-octave band spectrum analyzer. The analyzer determined sound pressure level spectra (referenced to 0.0002 microbar) between 50 and 20 000 Hz at each microphone position. A 4-second integration time was used. Three noise samples were taken at each microphone and treated statistically to reject background disturbances and random errors and to obtain either an average or a most probable value. The data were then corrected for atmospheric attenuation to give lossless data at 50 feet. From these sound pressure level spectra the overall sound pressure levels were calculated at each microphone location.

The combination of microphone height and distance from the model was selected (after a trial run in which they were varied) to give acceptable

cancellation and reinforcement amplitudes caused by ground reflections. The data of this report generally do not include ground reflection corrections except when making spectral comparisons. In these cases, ground reflection corrections to the SPL at each frequency were made by the method of Reference 11 which is an extension of the methods of References 12 and 13.

### Test Procedure

For each model configuration tested noise measurements were made for a series of nominal nozzle pressure ratios. These were 1.1, 1.2, 1.3, 1.4, 1.5, 1.7, and 1.8. The nozzle stagnation temperature varied between $55^{\circ}$ and $85^{\circ}$ F for the test series.

The exhaust velocities for each nominal pressure ratio setting were calculated from the measured values of nozzle pressure ratio and stagnation temperature. These velocities were used in the analysis of the acoustic data.

The exhaust plume of both the 13-inch conical nozzle and the coaxial nozzle was also surveyed with a total pressure rake in order to obtain radial velocity profiles at various axial locations along the nozzle centerline.

## Basis for Comparison of Data

### Correlation with Impingement Velocity

In order to obtain a basis for comparison of the data from the variety of configurations and test conditions employed, it is necessary to make some simplified generalizations about the sources of the flap noise. Blown flap interaction noise typically has a radiation pattern having two rather flat peaks located between $50^{\circ}$ and $80^{\circ}$ to each side of the flap exhaust direction (defined approximately by the trailing flap chordline). It will be assumed that this noise results from two principal components. One is an intense quadrupole noise emanating from the nozzle exhaust shear layer and from the exhaust fluid flowing adjacent to the flaps.[14-16] This turbulent mixing noise is intensified by the presence of solid surfaces in the exhaust flow. This quadrupole source has a directivity which peaks at an angle of about $20^{\circ}$ to $30^{\circ}$ with respect to the flap exhaust direction (similar to the data of Ref. 16). The other noise source is a strong dipole noise originating at the flap surfaces.[17-20] This source has a radiation pattern which peaks at approximately a $90^{\circ}$ angle with respect to the flap chordline direction. The overall sound pressure level will therefore show an exhaust velocity dependence between $V^8$ (quadrupole) and $V^6$ (dipole) depending on the microphone angle.

The dipole noise is dominant in the forward quadrant ($\theta = 0^{\circ}$ to $\theta = 90^{\circ}$) below the wing of a blown flap system, and because of its high intensity, usually provides the peak flyover noise. Therefore, the data

of this report will be examined and compared principally at microphone angles for which the dipole noise is dominant. In this region it is assumed that the RMS acoustic pressure, p, at a given microphone angle, $\theta$, can be represented by

$$p^2 \sim \left(\frac{\rho_o}{RC_o}\right)^2 \int_A I_i^2 V_i^6 \, dA \tag{1}$$

where R is the microphone distance, $\rho_o$ is the ambient density, $C_o$ is the ambient speed of sound, and the integral is based on the radial profiles of the jet impingement velocity, $V_i$, and the turbulent intensity, $I_i$, at the flap station, X.

For EBF systems having similar radial turbulent intensity profiles and having symmetrical single-peaked impingement velocity profiles at the flap impingement station, X, the integral of equation (1) can be approximated for scaling purposes by the technique used in Reference 16 to give the simplified relation

$$p^2 \sim \left(\frac{\rho_o}{RC_o}\right)^2 A_i V_{i,p}^6 \tag{2}$$

where $A_i = (\pi/4)d_i^2$ and $V_{i,p}$ is the peak impingement velocity obtained from the nozzle exhaust velocity profile at the flap station. The characteristic impingement diameter, $d_i$, is arbitrarily taken for scaling purposes as the width of the profile where the velocity is 80 percent of the peak impingement velocity. Both $V_{i,p}$ and $d_i$ are obtained from nozzle exhaust velocity radial profiles measured without the presence of the wing and flap system. The velocity profiles were calculated (assuming fully expanded isentropic flow) from the total pressure rake data.

The conical nozzle exhaust velocity decay data was found to be correlated within 1 percent by an expression of the form given in Reference 21. That is,

$$\frac{V_{i,p}}{V_N} = \left[1 + \left(\frac{0.14\ X}{D\sqrt{1 + M_N}}\right)^4\right]^{-1/4} \tag{3}$$

where X is the distance measured along the nozzle centerline from the exit plane to the point of intersection with the flap assembly (Figs. 1 to 3), D is the nozzle diameter, and $M_N$ is the nozzle exhaust Mach number. Equation (3) assumes an effective nozzle coefficient of 1.0, and the constant 0.14 was obtained from a fit of the rake data obtained in this investigation. Reference 21 gave a value of 0.15 for the constant based on small nozzle rake data.

The coaxial nozzle exhaust velocity decay data was found to be correlated by the expression (see Ref. 22 for a similar form)

$$\frac{V_{i,p}}{V_c} = \left\{1 + \left[\frac{0.14\,X}{D_C\sqrt{1 + M_c}\left(1 + \frac{V_F}{V_c}\right)^{0.875}}\right]^4\right\}^{-1/4} \tag{4}$$

where $D_C$ is the core diameter, $M_C$ is the core exhaust Mach number, $V_C$ is the core exhaust velocity, and $V_F$ is the fan (annulus) exhaust velocity. The exponent 0.875 for the term $(1 + V_F/V_C)^n$ was obtained from a recent unpublished NASA study, and the constant 0.14 is based on the rake data of this investigation.

Equations (3) and (4) were used to calculate $V_{i,p}$ for the comparisons of this paper. Values of $d_i$ were obtained directly from the measured velocity profiles. For special cases where either Equation (3) or (4) does not apply, normalized data from small-scale-model rake measurements taken at the Lewis Research Center were used.

Correlation with Nozzle Exhaust Velocity

In many instances, detailed exhaust velocity profile data or complete correlations for $V_{i,p}$ and $d_i$ are not available for making comparisons or predictions of flap noise. In these cases it is necessary to compare data and/or make predictions using nozzle exhaust velocity and area as parameters. However, such an approach is applicable only for nozzles with low velocity decay (nonmixer type) or for nozzles with similar decay characteristics. For these cases, data can be compared by using an effective nozzle exhaust velocity, $V_E$, and total exhaust nozzle exit area, $A_T$. The effective exhaust velocity is obtained by evaluating the velocity profile integral of equation (1) at the nozzle exhaust exit planes (instead of at the flap station). That is,

$$\int_A V^6\,dA = A_T V_E^6 = A_C V_C^6 + A_F V_F^6 \tag{5}$$

where

$$A_T = A_C + A_F \tag{6}$$

and

$$V_E = \left(\frac{A_C V_C^6 + A_F V_F^6}{A_T}\right)^{1/6} \tag{7}$$

For single conical (round convergent) nozzles, $V_E = V_N$ where $V_N$ is the nozzle exhaust velocity and $A_T$ simply becomes, $A_N$, the nozzle exit area. Equation (7) was used in the simplified flap noise prediction method of reference 23. The use of equation (7) assumes that the velocity decay and spreading characteristics of the EBF systems which are being compared are comparable and that the differences that do exist will have only a secondary effect on the flap noise. This approach amounts to the approximation that

$$A_T V_E^6 \sim A_i V_{i,p}^6 \tag{8}$$

or in terms of RMS acoustic pressure at angle, $\theta$

$$p^2 \sim \left(\frac{\rho_o}{RC_o}\right)^2 A_T V_E^6 \tag{9}$$

Normalization to Standard Day Source

The RMS acoustic pressure is dependent on the ambient density and ambient speed of sound (Eq. (2) and (9)). These quantities in turn are dependent on the ambient temperature and pressure at the time of the sound measurements. The data of this report were therefore normalized to Standard Day noise source conditions. It should be pointed out that the Standard Day normalization procedure did not involve the customary atmospheric attenuation corrections inasmuch as all sound data herein were previously corrected for losses due to atmospheric absorption and are therefore lossless. In terms of OASPL the data were converted to Standard Day conditions by the following relation

$$OASPL_{STD} = OASPL_O + 10 \log\left(\frac{T_O}{T_{STD}}\right)^3\left(\frac{P_{STD}}{P_O}\right)^2$$

where

$$T_{STD} = 519^o \text{ R}$$

$$P_{STD} = 29.92 \text{ in. of Hg}$$

and $T_O$ and $P_O$ are the ambient temperature and pressure on the day of the test.

Although the Standard Day correction was usually less than ±0.6 dB and did not exceed ±1.0 dB in extreme cases, it was found that this correction did reduce data scatter which in turn allowed other weak effects to be observed.

## Results and Discussion

The results of the acoustic tests of the externally blown flap models listed in Table 1 will be discussed in terms of the effect of configuration variation on flap noise radiation patterns (directivity), spectral shape, and sound pressure level.

### Effect on Noise Radiation Patterns

Flap noise radiation patterns at a 50-foot radius are shown in polar form in Figure 7 for selected configurations having a trailing flap angle of $60^{\circ}$. Figure 7(a) shows normalized overall sound pressure level (OASPL-10 log $A_T$) as a function of microphone angle, for three 13-inch-conical nozzle configurations (#6, #9, and #10 of Table 1) and the plug-nozzle configuration (#12). The nozzle exhaust velocity was 765 ft/sec for the four cases. The nozzle exit area, $A_T$, was normalized to 1 $ft^2$. The four radiation patterns are similar with only minor differences in directivity evident. Configurations #6 and #10 both have the OASPL radial peak located in the forward quadrant below the wing at $\theta = 40^{\circ}$. This is not surprising as the models were designed to expose the two lower flaps of the 3-flap wing (config. #10) to the same exhaust flow profile as the baseline two-flap wing (config. #6). The baseline three-flap configuration (#9) is a little louder and peaks at $55^{\circ}$. The plug-nozzle configuration also has a radial peak at $55^{\circ}$ at this velocity (at lower velocity the peak occurs at $40^{\circ}$). The microphone angle, $\theta$, producing a flyover maximum is $70^{\circ}$ for all four cases.

Radiation patterns for three coaxial nozzle configurations having a $60^{\circ}$ trailing flap angle (#1, #4, and #5 of Table 1) are shown in Figure 7(b). The effective exhaust velocity was 655 ft/sec. The baseline 2-flap configuration (#1) and the 3-flap configuration with Y = 29.25 in. (#5) both have peak radial values of OASPL at $40^{\circ}$. Again this was not unexpected because, like 13 in.-conical-nozzle configurations #6 and #10, these coaxial models were designed so that the lower two flaps of the 3-flap model (#5) would have the same impingement velocity distribution over their surfaces as the baseline 2-flap model (#1). The baseline three-flap model (#4) has a radial peak at $55^{\circ}$. All three configurations had a flyover maximum at $\theta = 70^{\circ}$.

In summary, the data in Figure 7 show that configuration variations such as nozzle type or the number of flaps had only a minor effect on the radiation pattern. The radiation pattern was actually somewhat more sensitive to nozzle exhaust velocity. For velocities above 900 ft/sec, the polar peak occurred at about $70^{\circ}$ and rotated to $40^{\circ}$ for the baseline 2-flap model and to $55^{\circ}$ for the baseline 3-flap models as the exhaust velocity was lowered to levels below 800 ft/sec. This effect occurs because as the velocity is lowered, the dipole noise becomes increasingly more dominant in this region (in comparison with the quadrupole mixing noise).

Effect on Spectral Shape

In general, except for changes in trailing flap angle, the effects of configuration changes on the measured 1/3-octave SPL spectra at a given microphone location were small. No striking changes were noted in either the spectral shape or in the location of the peak frequency. The peak frequency, of course, did shift with nozzle diameter according to the Strouhal relation as previously discussed in References 3 and 24. The largest effect occurred with change in trailing flap angle where it was noted that the peak in the flap noise spectrum shifted towards lower frequency as the trailing flap angle was decreased. The configurations with a $20^{\circ}$ trailing flap angle tended to peak at a Strouhal number which was roughly one-half that of the $60^{\circ}$ trailing flap configurations.

In order to make detailed comparisons of spectral shapes measured for different configurations, it was necessary to correct the SPL spectra for ground effects. This was done for a limited number of spectra for the baseline models. The resulting approximate free field SPL data were then converted to normalized SPL spectral density (SPL - OASPL + 10 log $(V_E/D_T)$ - 10 log $\Delta f$) and plotted against the Strouhal number $(fD_T/V_E)$ as shown in Figures 8 and 9 for the $70^{\circ}$ microphone angle. Each curve shown in Figures 8 and 9 was obtained by fairing through a set of points calculated from data for five different effective exhaust velocities in the range of 450 to 1000 ft/sec. The $70^{\circ}$ angle was chosen because it yields the flyover maximum flap noise, as pointed out in the previous section.

The effect of the number of flaps on the spectral shapes for the baseline models having a $60^{\circ}$ trailing flap angle (Figs. 1, 2(b), and 3(b)) is shown in Figure 8. The 13-inch conical nozzle configurations (#6 and #9 of Table 1) are compared in Figure 8(a). The spectral shapes of Figure 8(a) are generally similar, with the 2-flap spectrum being somewhat broader and less peaked than the 3-flap data. The coaxial nozzle configurations (#1 and #4) compared in 8(b) show similar trends.

The effect of nozzle type on the spectra for given flap configurations is shown in Figure 9. The two-flap data are compared in Figure 9(a) and the three-flap data are compared in Figure 9(b). Figure 9 shows that the type of nozzle employed (conical or coaxial) did not change the spectral shape. Although the curves are displaced, the shape of the spectra for both the two-flap and three-flap models were very similar for the two types of nozzles. The displacement of the spectra for the conical and coaxial configurations shows that $V_E$ and $D_T$ are not the best scaling parameters to use when comparing spectra from EBF configurations having different types of nozzles. Improvement can be made by correlating the data in terms of exhaust-jet impingement parameters.

When the 3-flap data used in Figure 9(b) are compared using the impingement parameters $V_{i,p}$ and $d_i$ to calculate the normalized SPL spectral density and Strouhal number instead of the nozzle parameters $V_E$ and $D_T$, the correlation of the data is considerably improved as shown in

Figure 10. Data are shown for two values of impingement velocities for the coaxial nozzle configuration (Fig. 3(b)) and for the 13-in. convergent nozzle configuration (Fig. 2(b)). The scatter in the low frequency peak region is caused primarily by lack of precision in applying ground corrections to the data. The ground effect causes strong cancellations and reinforcements in this part of the spectra and the present state of the art does not lend itself to accurate calculation of ground effect corrections. However, the general overall improvement along with the good correlation at mid-frequencies ($fd_i/V_{i,p}$ = 0.8 to 4.0) indicates that the use of $V_{i,p}$ and $d_i$ as scaling parameters considerably improves the correlation of the spectral data.

## Effect on Overall Sound Pressure Level

Correlation with Nozzle Exit Parameters. Normalized overall sound pressure level (OASPL - 10 log $A_T$) for the 70° microphone is plotted in Figure 11 as a function of the effective nozzle exhaust velocity for four two-flap EBF configurations with a 60° trailing flap angle but having different kinds of exhaust nozzles (configs. #1, #6, #11, and #12 of Table 1). It is clear from Figure 11 that while the OASPL for the flap noise is dependent on nozzle exit area and on effective exhaust velocity, it is not dependent on nozzle type. The data for the conical, plug, and coaxial nozzle EBF configurations are correlated quite well by the use of nozzle area and exhaust velocity parameters alone. It should be noted that the slope of the curve drawn through the data indicates a velocity power exponent of about 6.7 rather than the theoretical value of six given by Equation (9).

The normalized overall sound pressure levels measured at the microphone angle corresponding to the radial peak value for each of the four 2-flap configurations of Figure 11 plus the swept-wing 2-flap configuration (Fig. 5) are plotted in Figure 12 against effective nozzle exhaust velocity. The OASPL data are plotted for the microphone angle corresponding to the radial peak in Figure 12 because the dipole noise component of the flap noise should be strongest at the radial peak. The data are again well correlated in terms of $A_T$ and $V_E$. However, even at this microphone angle the OASPL does not vary with the sixth power of the effective nozzle exhaust velocity. The exponent is again about 6.7 as noted for the data of Figure 11.

The effective exhaust velocity was defined for the 16° swept wing configuration as $V_E = V_N \cos 16°$. In general at a given $V_N$ the swept wing configuration (Fig. 5) was 1 to 2 dB quieter than the corresponding unswept configuration. Figure 12 shows that using the component of velocity perpendicular to the line defined by the flap leading edge correlates the data reasonably well with that for the unswept EBF configurations.

The normalized OASPL data for the baseline (Y = 19.25 in.) and the low-nozzle-position (Y = 29.25 in.) three-flap configurations are compared in Figure 13 at the microphone angles corresponding to a flyover

maximum in each case. Data are shown for configurations having trailing flap angle settings of 20° (takeoff) and 60° (landing) and are plotted against effective exhaust velocity. The data for the 13-inch conical nozzle three-flap configurations (#7, #8, #9, and #10) are compared in Figure 13(a). The coaxial nozzle 3-flap configurations (#2, #3, #4, and #5) are compared in Figure 13(b).

Figure 13(a) shows that for the baseline configuration there is about a 1.5 dB increase in OASPL when the flaps are lowered from the 20° to the 60° trailing flap position. However, with the low-nozzle-position there is a much larger difference in noise level for the two flap positions. The 20° flap position is much quieter (about 8 dB) for this configuration because the nozzle centerline axis passes just below the trailing edge of the last flap resulting in over half of the exhaust jet missing the flap system. In addition, the impingement distance for this case has increased by 14 inches over the baseline case (Table 1). With 60° trailing flaps, the data in Figure 13(a) show that lowering the nozzle 10 inches caused only a small decrease in noise level (about 2 dB). For the 60° case the impingement distance did not change and the exhaust capture area changed a relatively small amount.

The coaxial nozzle configuration data of Figure 13(b) show the same general trends as 13(a), but the upper three curves are somewhat closer together. This relative insensitivity to geometry changes suggests that there is slightly more wing scrubbing noise with the coaxial nozzle configurations. The large decrease in noise (about 8 dB for the 20° flap angle setting with the nozzle in the low position (Y = 29.25 in.) occurs for the same reasons as discussed for the corresponding 13-inch conical nozzle data of Figure 13(a).

Correlation with Impingement Parameters. Normalized overall sound pressure level (OASPL - 10 log $A_i(50/R)^2$) for 2-flap configurations (#6, #11, and #12) with single-element nozzles (conical and plug) and 60° trailing flap position are plotted at the angle corresponding to the radial peak value as a function of the peak impingement velocity, $V_{i,p}$, in Figure 14. Also shown are data from Reference 4 for a small scale model (2-in. diameter nozzle) of configuration 1 of Table 1. It should be noted that the OASPL in Figure 14 is normalized using the impingement area, $A_i$ (normalized to 1 $ft^2$), as the area parameter instead of the nozzle exhaust exit area as in Figures 11, 12, and 13. The microphone radius term $(50/R)^2$ was included because the small scale data were measured at 10 ft instead of 50 ft. Figure 14 shows that the parameters $A_i$ and $V_{i,p}$ correlate the single-element nozzle data very well. Further the data can now be fitted by a 6th power of velocity curve instead of the 6.7 power required to fit the data using nozzle exhaust parameters. Thus, the use of impingement parameters in the correlation gives very good agreement with the simple dipole source model (Eq. (2)).

OASPL data are compared in Figure 15 for the two coaxial and two conical nozzle EBF configurations having (for each nozzle type) similar impingement velocity profiles at the two lower flaps. It is immediately

apparent that the data for the coaxial nozzle configurations are displaced from the conical nozzle data. The coaxial nozzle data are about 3.5 dB quieter. This difference is significant and probably results from basic differences in the nozzle exhaust shear layer turbulence intensity radial profiles at the flap station for single element and coaxial nozzles. Thus, in order to correlate the coaxial and conical nozzle data the ratio of the respective turbulence intensity and impingement velocity product integrals of Equation (1) is needed.

The coaxial nozzle exhaust jet characteristics are basically treated herein in terms of the core jet flow (e.g., Eq. (4)). The surrounding annular flow from the fan nozzle is assumed primarily to modify the velocity decay, spreading, and turbulence characteristics of the central core jet. Thus, for coaxial nozzles having fan-to-core velocity ratios significantly less than 1.0 (say, about 0.85) the turbulent intensity will be assumed to be a function of the relative velocity between the core and the fan (annulus) exhausts. If it is assumed that the flap noise reduction observed in free-jet relative velocity tests of EBF models[8] is primarily due to a reduction in turbulence intensity, then an empirical expression for approximating this function can be obtained.

Based on examination of data from recent free-jet relative velocity effect tests at the Lewis Research Center and on limited ($V_F/V_C = 0.8$ case only) nozzle exhaust plume turbulence data at the flap station, the following empirical relation was obtained for the relative overall sound pressure levels between conical and coaxial nozzle EBF configurations:

$$OASPL_{(conv.)} = OASPL_{(coaxial)} - 6 \log\left(\frac{V_C - V_F}{V_C}\right) \tag{10}$$

By adopting the convention that $V_F = 0$ for a conical nozzle, the parameter on the right can be used as a general normalization term to account for turbulence intensity (or turbulent mixing) differences for the two classes of nozzles.

Coaxial nozzles with $V_F/V_C > 0.85$ require special treatment because as the ratio $V_F/V_C$ approaches unity, the coaxial nozzle exhaust profile spreading characteristics, decay rate, and turbulence intensity at the flap station, X, become increasingly similar to those for a conical nozzle. This results from the fact that with $V_F/V_C = 1.0$, the fan and core exhaust streams combine rapidly with axial distance to form a single circular exhaust jet.

Data for the coaxial and conical nozzle EBF configurations of Figure 15 are compared in Figure 16 using the empirical parameter, $6 \log(1 - V_F/V_C)$ as well as $A_i$ to normalize the OASPL. Inclusion of this term as a parameter results in a good 6th power correlation of the data for the two types of nozzles based on $V_{i,p}$. Coaxial nozzle 3-flap configuration data for tests where the ratio $V_F/V_C = 1.0$ are also included in the figure using separate symbols for the data points.

With the nozzle effects correlated it is possible to isolate the effect of the number of flaps in an EBF configuration on the noise level. Radial peak values of the normalized OASPL for baseline 2- and 3-flap configurations having conical and coaxial nozzles are shown in Figure 17. The parameter $6 \log(1 - V_F/V_C)$ is used along with $A_i$ and $V_{i,p}$ to correlate the data. The correlations show that with the trailing flap at an angle of $60^\circ$, the difference between the 2- and 3-flap data is only about 1 to 1.5 dB. Thus with the baseline configurations of this report the addition of the third flap had only a small effect on the OASPL.

Comparison with Engine EBF Data

In this section the flap noise data from the cold-flow model tests reported herein will be compared with similar data obtained from tests employing a turbofan engine to blow the flaps. By doing this it is possible to assess the importance of real engine effects such as exhaust plume temperature on the flap noise sound field. Previously it was shown[23] that the 2-flap cold-flow model of Reference 3 gave generally similar results to those measured in EBF tests using a three-flap wing section blown by the exhaust from a high bypass ratio, highly noise suppressed turbofan engine.[8,25,26] The baseline coaxial 3-flap configuration of this report (Fig. 3) is geometrically very similar to the baseline turbofan engine EBF test configuration of Reference 26 (shown in Fig. 18) and is roughly one-half scale.

Normalized SPL spectral density (SPL - OASPL + 10 log $V_E/D_T$ - 10 log $\Delta f$) curves for the microphone yielding the flyover maximum in each test are compared in Figure 19. The engine data are for the $55^\circ$ trailing flap angle position (Fig. 18), and the baseline 3-flap coaxial data are for the $60^\circ$ position (Fig. 3(b)). The engine data are for the $80^\circ$ microphone and the cold flow model data are for the $70^\circ$ microphone. Both sets of one-third octave SPL data were corrected for ground effects. Figure 19 shows that the spectral shapes are very similar.

The normalized OASPL is plotted against $V_E$ in Figure 20(a) for the microphone angles corresponding to the flyover maximum for the engine and cold-flow model tests. Data for landing flap angle settings are given. With the exception of the data point for the lowest velocity (low fan speed) engine test the data are correlated by about the 6.7 power of effective nozzle exhaust velocity.

Thus Figures 19 and 20(a) show that $V_E$ and $D_T$ (or $A_T$) correlate the data for the two coaxial-nozzle EBF tests quite well, as pointed out in Reference 23, even though the ratio $V_F/V_C$ varied in a different manner with change in core velocity for the two systems. For the engine tests, the fan to core velocity ratio, $V_F/V_C$, varies from 0.78 at 100 percent fan speed to 1.02 at low fan speed. For the model data shown, $V_F/V_C$ varied from 0.865 at high velocity to 0.769 at low velocity.

Since both the peak impingement velocity of a coaxial nozzle (see Eq. (4)) and the impingement area depend on the ratio $V_F/V_C$, it is

reasonable to expect that the exhaust impingement parameters $V_{i,p}$ and $A_i$ would be a somewhat better choice for correlating the data. Engine exhaust-plume velocity profiles were measured in the tests reported in Reference 26. This data was employed to determine $V_{i,p}$ and $A_i$ for the engine flap noise data shown in Figure 20(b). In Figure 20(b) the normalized OASPL is plotted against $V_{i,p}$. Figure 20(b) shows that the cold-flow model and real engine EBF tests produced very similar OASPL levels for the flap noise and are correlated by the 6th power of the peak impingement velocity.

The flap noise radiation patterns for the engine and the cold-flow model tests are compared in Figure 21 at constant peak impingement velocity. Comparisons are made at $V_{i,p}$ values of 751 and 527 ft/sec. As in Figure 20(b), the OASPL is normalized by using the impingement area, $A_i$, as a parameter. The flap noise data are compared in the forward quadrant below the wing ($\theta = 0^o$ to $90^o$) where the low frequency dipole noise makes the major contribution to the OASPL.

The good agreement between the model and the engine data of Figure 21 indicates that exhaust plume temperature has little effect on the flap noise directivity pattern. This effect is not surprising because the most intense dipole noise is radiated from the flaps nearly at right angles to the local exhaust flow direction and thus convection and refraction effects would be expected to be small in the peak flap noise region.

The data of Figures 19, 20, and 21 indicate that for the configurations tested exhaust plume temperature and other real engine effects did not appear to be important factors in determining flap noise level, directivity, and spectral shape. Thus cold-flow, scale-model tests of EBF systems may be used to predict the flap noise contribution to the overall noise of a full scale EBF system employing a turbofan engine.

## Summary of Results

The flap noise data of this investigation were correlated in terms of two different sets of nozzle exhaust-jet parameters with the following results:

(1) The OASPL data for flaps blown by conical and plug nozzles could be correlated by using nozzle exhaust velocity and nozzle exit area as parameters.

(2) For coaxial exhaust nozzles, the data were correlated by using the total (core + fan) nozzle exit area, $A_T$, and a 6th power weighted nozzle exhaust velocity, $V_E$, obtained from

$$V_E = \left( \frac{V_F^6 A_F + V_C^6 A_C}{A_T} \right)^{1/6}$$

(3) The flap noise level was proportional to about the 6.7th power of the effective exhaust velocity for all nozzle types.

(4) Better correlation of OASPL data could be obtained by using the peak impingement velocity and the impingement area (jet cross section) at the flap station. To correlate coaxial with conical nozzle configurations an additional parameter was required to account for differences in turbulence intensity.

(5) The flap noise level was found to be proportional to the 6th power of the flap impingement velocity in all cases.

The sensitivity to configuration (or geometry) variations can be summarized as follows:

(1) For the nozzles tested (conical, plug, and coaxial), the effect of nozzle type on the flap noise level, spectra, and directionality was found to be negligible.

(2) Variations in flap geometry (other than trailing flap angle) such as 2-flap versus 3-flap systems generally had only a small effect on EBF spectral shape, noise level (about 1.5 dB), and noise radiation pattern.

(3) Other things being equal, the spectrum for the 2-flap system was somewhat broader and less peaked than the spectrum for the 3-flap system.

(4) The effect of a $16^{\circ}$ sweep-back of the wing on OASPL was found to be small (~2 dB).

(5) With the trailing flap at the $60^{\circ}$ position, lowering the nozzle from $19\frac{1}{4}$ to $29\frac{1}{4}$ inches below the wing decreased the OASPL by $1\frac{1}{2}$ to 2 dB.

The comparison of the cold-flow model EBF data of this investigation with limited flap noise data from geometrically similar EBF tests using a highly noise-suppressed turbofan engine indicated the following:

(1) The normalized SPL spectral density versus the Strouhal number curve and the OASPL radiation pattern in the forward quadrant obtained with the cold-flow 3-flap model are nearly the same as obtained with flaps blown by the turbofan engine.

(2) These results suggest that exhaust plume temperature does not appear to be an important factor in determining flap noise overall sound pressure level, directivity, or spectral shape in the forward quadrant below the wing. It appears, therefore, that cold-flow scale-model test data can be used to predict the flap noise for a full scale EBF system using a turbofan engine.

## References


1. Maglieri, D. J. and Hubbard, H. H., "Preliminary Measurements of the Noise Characteristics of Some Jet-Augmented-Flap Configurations", Memo 12-4-58L, Jan. 1959, NASA.

2. Dorsch, R. G., Krejsa, E. A., and Olsen, W. A., "Blown Flap Noise Research," AIAA Paper 71-745, Salt Lake City, Utah, 1971.

3. Dorsch, R. G., Kriem, W. J., and Olsen, W. A., "Externally-Blown-Flap Noise," AIAA Paper 72-129, San Diego, Calif., 1972.

4. Olsen, W. A., Dorsch, R. G., and Miles, J. H., "Noise Produced by a Small-Scale, Externally Blown Flap," TN D-6636, March 1972, NASA.

5. Gibson, F. W., "Noise Measurements of Model Jet-Augmented Lift Systems," TN D-6710, Apr. 1972, NASA.

6. Putnam, T. W., and Lasagna, P. L., "Externally Blown Flap Impingement Noise," AIAA Paper 72-664, Boston, Mass., 1972.

7. Falarski, M. D., Aoyagi, K., and Koenig, D. G., "Acoustic Characteristics of Large-Scale STOL Models at Forward Speed," STOL Technology, NASA SP-320, Moffett Field, Calif., Oct. 1972, pp. pp. 443-454.

8. Dorsch, R. G., and Reshotko, M., "EBF Noise Tests with Engine Under-the-Wing and Over-the-Wing Configurations," STOL Technology, NASA SP-320, Moffett Field, Calif., Oct. 1972, pp. 455-461.

9. Dorsch, R. G., Reshotko, M., and Olsen, W. A., "Flap Noise Measurements For STOL Configurations Using External Upper Surface Blowing," AIAA Paper 72-1203, New Orleans, La., 1972.

10. Reshotko, M., Goodykoontz, J. H., and Dorsch, R. G., "Engine-Over-The-Wing Noise Research," AIAA Paper 73-631, Palm Springs, Calif., 1973.

11. Miles, J. H., "Rational Function Representation of Flap Noise Spectra With Application to Correcting For Reflection Effects," AIAA Paper 74-193, Washington, D.C., 1974.

12. Howes, W. L., "Ground Reflection of Jet Noise," TR R-35, 1959, NASA.

13. Thomas, P.,"Acoustic Interference by Reflection: Application to the Sound Pressure Spectrum of Jets," Aircraft Engine Noise and Sonic Boom, AGARD-CP- 42, Saint-Louis, France, May 1969.

14. Phillips, O. M., "On the Aerodynamic Surface Sound from a Plane Turbulent Boundary Layer," Proceedings of the Royal Society (London), Series A, Vol. 234, No 1198, Feb. 21, 1956, pp. 327-335.

15. Powell, A., "Aerodynamic Noise and the Plane Boundary", Journal of the Acoustical Society of America, Vol. 32, No. 8, Aug. 1960, pp. 982-990.

16. Olsen, W. A., Miles, J. H., and Dorsch, R. G., "Noise Generated by Impingement of a Jet Upon a Large Flat Board", TN D-7075, Dec. 1972, NASA.

17. Curle, N., "The Influence of Solid Boundaries on Aerodynamic Sound", Proceedings of the Royal Society (London), Series A., Vol. 231, No. 1187, Sept. 20, 1955, pp. 505-514.

18. Hayden, R. E., "Noise From Interaction of Flow With Rigid Surfaces: A Review of Current Status of Prediction Techniques," CR-2126, Oct. 1972, NASA.

19. Hersh, A. S. and Hayden, R. E., "Aerodynamic Sound Radiation From Lifting Surfaces With and Without Leading-Edge Serrations," NASA CR-114370, 1971, Bolt, Beranek, and Newman, Inc., Canoga Park, Calif.

20. Fink, M. R., "Mechanisims of Externally Blown Flap Noise," AIAA Paper 73-1029, Seattle, Wash., 1973.

21. von Glahn, U. H., Groesbeck, D. E., and Huff, R. G., "Peak Axial-Velocity Decay With Single- And Multi-Element Nozzles," AIAA Paper 72-48, San Diego, Calif., 1972.

22. von Glahn, U., Sekas, N., Groesbeck, D., and Huff, R., "Forward Flight Effects on Mixer Nozzle Design and Noise Considerations for STOL externally Blown Flap Systems, AIAA Paper 72-792. Los Angeles, Calif., 1972.

23. Clark, B. J., Dorsch, R. G., and Reshotko, M., "Flap Noise Prediction Method For A Powered Lift System", AIAA Paper 73-1028, Seattle, Wash., 1973.

24. Dorsch, R. G., Lasagna, P. L., Maglieri, D. L., and Olsen, W. A., "Flap Noise," Aircraft Engine Noise Reduction, NASA SP-311, Cleveland, Ohio, May 1972, pp. 259-290.

25. Jones, W. L., Heidelberg, L. J., and Goldman, R. G., "Highly Noise-Suppressed Bypass 6 Engine for STOL Applications," AIAA Paper 73-1031 Seattle, Wash., 1973.

26. Samanich, N. E., Heidelberg, L. J., and Jones, W. L., "Noise Investigation of a Full-Scale Externally Blown Flap System with a Quiet 6:1 Bypass Ratio Engine and a Three-Flap Wing Section," AIAA Paper 73-1217, Las Vegas, Nev., 1973.

Table 1 EBF test configurations[1]

| Configuration number | Model | Flap angles (deg) | X (in.) | Y (in.) | $\frac{X}{D_C}$ | $\frac{X}{D_T}$ |
|---|---|---|---|---|---|---|
| Coaxial nozzle: ($A_T$ = 1.54 ft$^2$, $D_T$ = 1.40 ft, $D_C$ = 0.68 ft) | | | | | | |
| 1* | 2-flap | 30-60 | 72 | 19.25 | 8.8 | |
| 2* | 3-flap | 13-15-20 | 72 | 19.25 | 8.8 | |
| 3 | | 13-15-20 | 86 | 29.25 | 10.5 | |
| 4* | | 3-50-60 | 72 | 19.25 | 8.8 | |
| 5 | | 3-50-60 | 72 | 29.25 | 8.8 | |
| 13-in. diameter conical nozzle: ($A_T$ = 0.922 ft$^2$, $D_T$ = 1.08 ft) | | | | | | |
| 6* | 2-flap | 30-60 | 94 | 19.25 | | 7.2 |
| 7* | 3-flap | 13-15-20 | 94 | 19.25 | | 7.2 |
| 8 | | 13-15-20 | 108 | 29.25 | | 8.3 |
| 9* | | 3-50-60 | 94 | 19.25 | | 7.2 |
| 10 | | 3-50-60 | 94 | 29.25 | | 7.2 |
| 8-in. diameter conical nozzle: ($A_T$ = 0.36 ft$^2$, $D_T$ = 0.68 ft) | | | | | | |
| 11 | 2-flap | 30-60 | 72 | 19.25 | | 8.8 |
| 23.25-in. diameter plug nozzle: ($A_T$ = 1.18 ft$^2$, $D_T$ = 1.23 ft) | | | | | | |
| 12 | 2-flap | 30-60 | 94 | 19.25 | | 6.4 |
| 13-in. diameter conical nozzle with 16° wing sweep | | | | | | |
| 13 | 2-flap | 30-60 | 72 | 19.25 | | 7.2 |
| Coaxial nozzle with screen removed ($V_F/V_C$ = 1.0) | | | | | | |
| 14 | 3-flap | 3-50-60 | 72 | 29.25 | | 4.3 |

[1] Notation defined in Symbols section.

* Baseline configurations (Figs. 1 to 3).

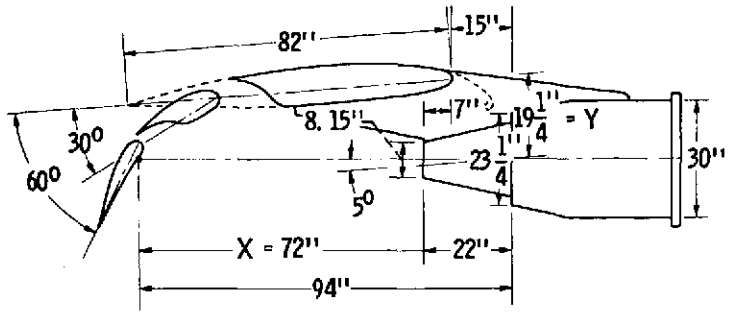


(a) WITH PYLON MOUNTED COAXIAL NOZZLE. (CONFIG. #1 OF TABLE I.)

CS-68879

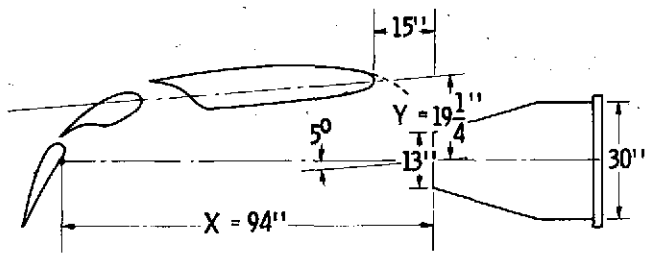


(b) WITH 13-IN.-DIAM CONICAL NOZZLE. (CONFIG. #6 OF TABLE I.)

CS-68878

Figure 1. - Baseline 2-flap EBF configurations.

E-7858

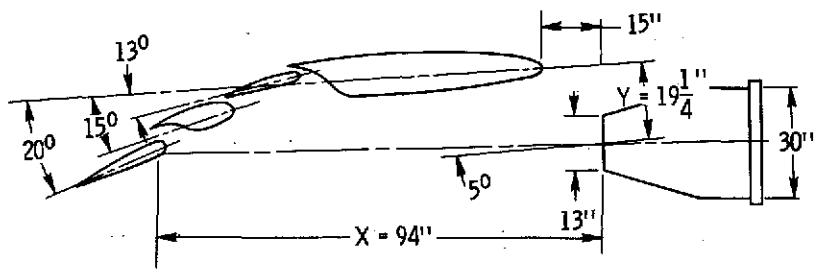


(a) WITH 20° TRAILING FLAP POSITION. (CONFIG. #7 OF TABLE I.)

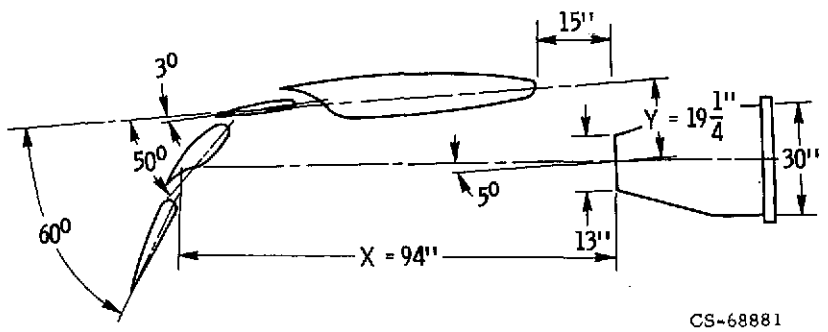


CS-68881

(b) WITH 60° TRAILING FLAP POSITION. (CONFIG. #9 OF TABLE I.)

Figure 2. - Baseline 3-flap EBF configuration with 13-inch-diameter conical nozzle.

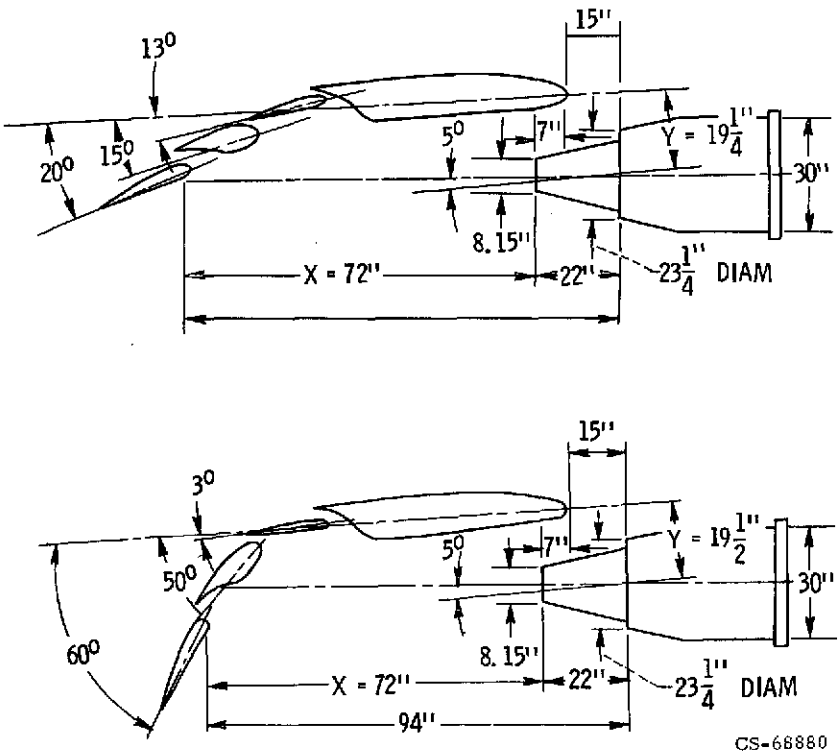


Figure 3. - Baseline 3-flap EBF configuration with coaxial nozzle.

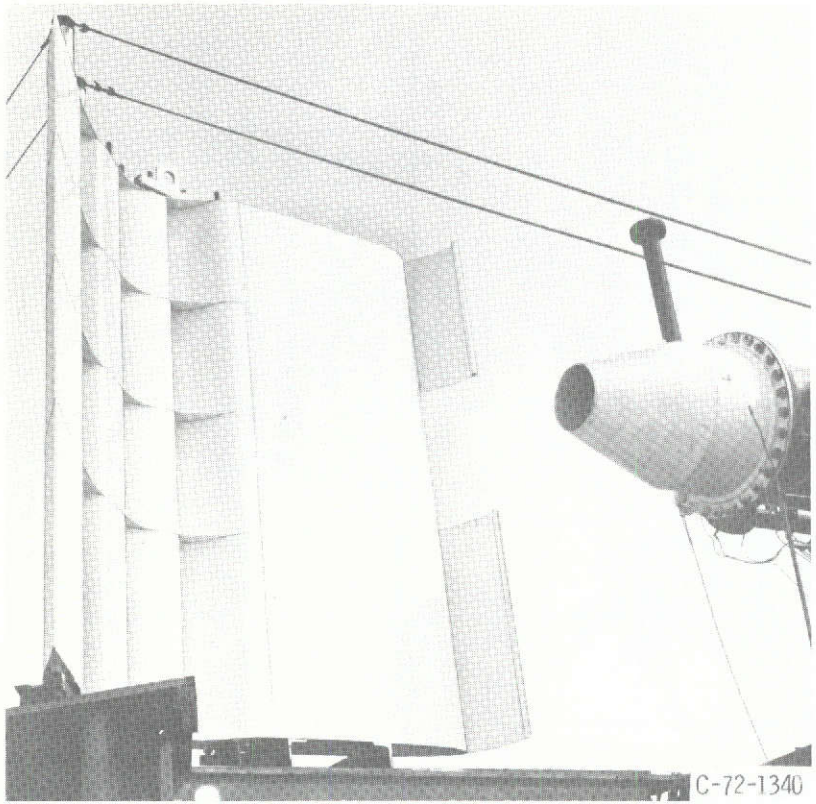


(a) WITH 13-INCH-DIAMETER CONICAL NOZZLE.

Figure 4. - Three-flap externally blown flap model.

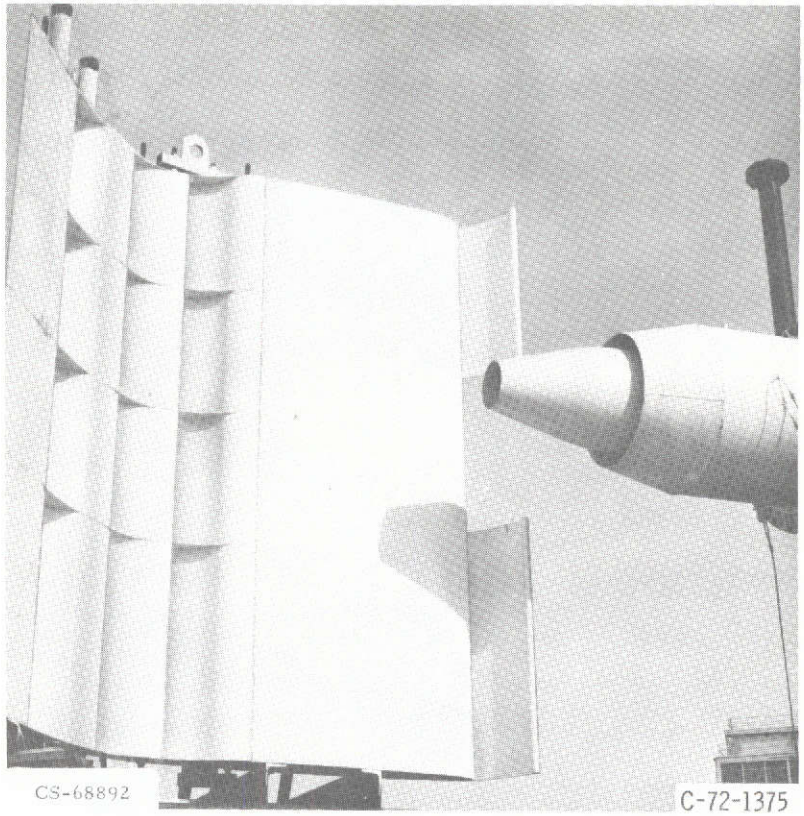


(b) WITH COAXIAL NOZZLE.

Figure 4. - Concluded.

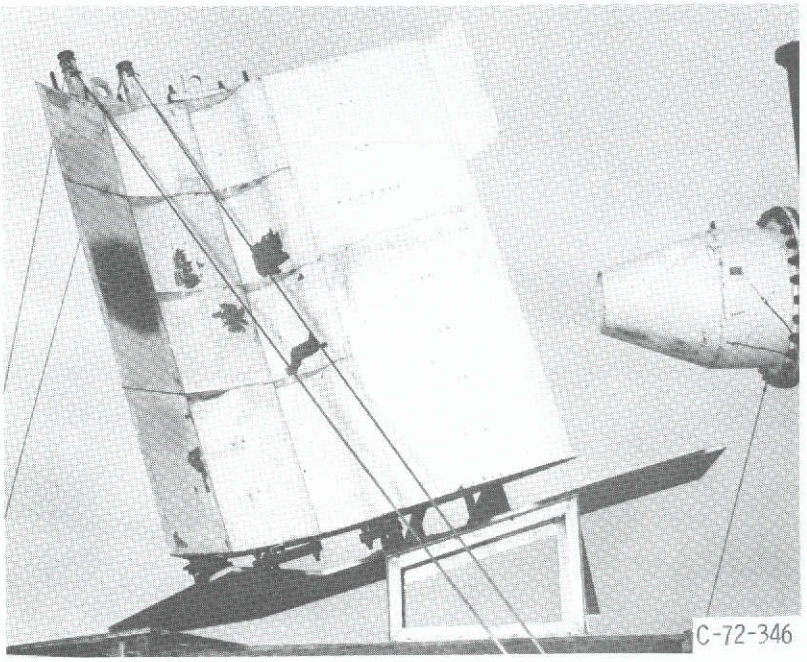


Figure 5. - Two-flap EBF model with 16 degree wing sweep-back.

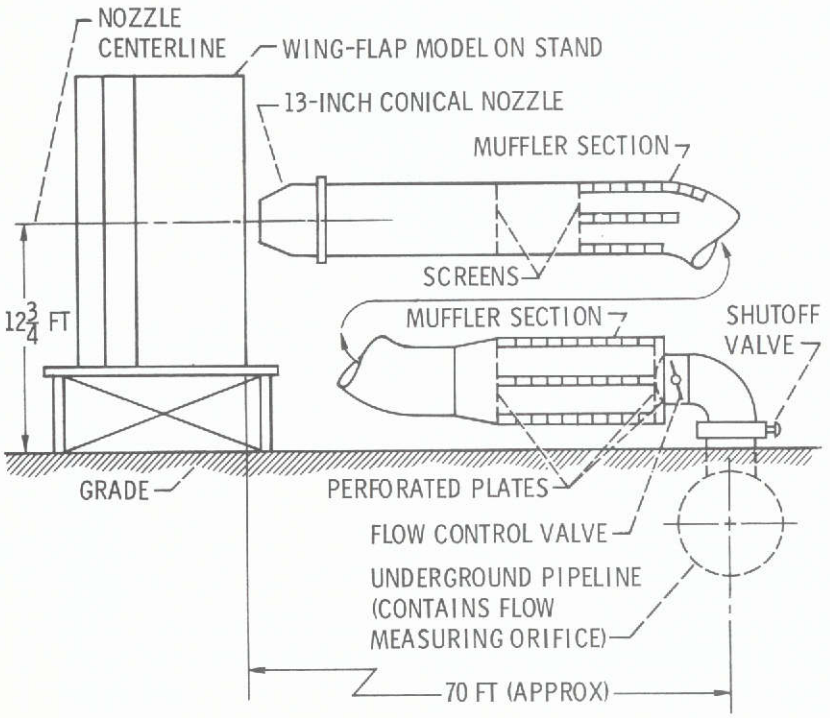


Figure 6. - Nozzle air supply system.

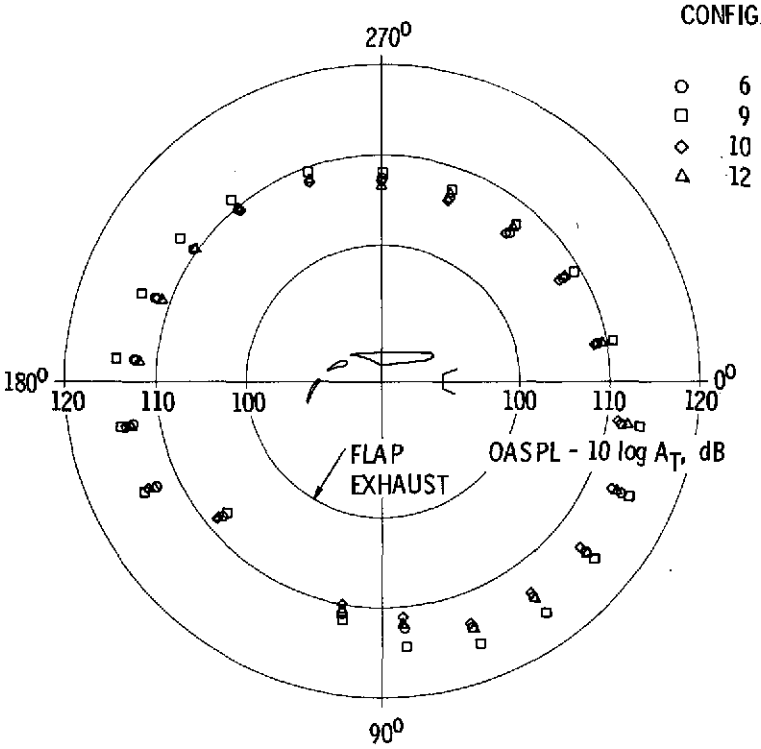


| CONFIG. # | FLAPS | Y, IN. | NOZZLE |
|---|---|---|---|
| ○ 6 | 2 | 19.25 | 13-IN. CONICAL |
| □ 9 | 3 | 19.25 | 13-IN. CONICAL |
| ◇ 10 | 3 | 29.25 | 13-IN. CONICAL |
| △ 12 | 2 | 19.25 | PLUG |

CS-68891

(a) 13-IN. DIAMETER CONICAL NOZZLE AND PLUG NOZZLE CONFIGURATIONS. NOZZLE EXHAUST VELOCITY, 765 FT/SEC.

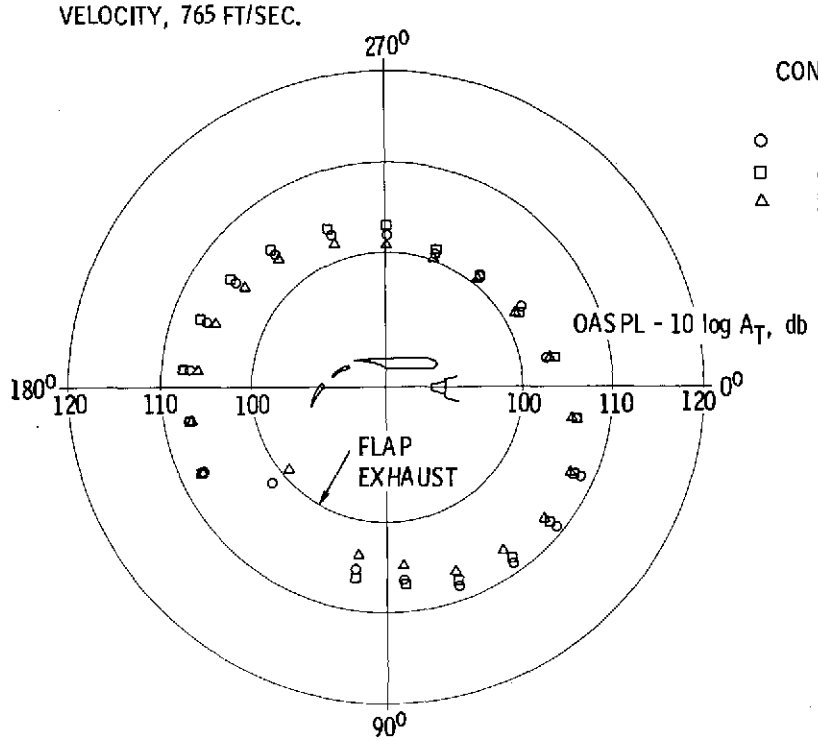


| CONFIG.# | FLAPS | Y, IN. |
|---|---|---|
| ○ 1 | 2 | 19.25 |
| □ 4 | 3 | 19.25 |
| △ 5 | 3 | 29.25 |

(b) COAXIAL NOZZLE CONFIGURATIONS. EFFECTIVE NOZZLE EXHAUST VELOCITY, 655 FT/SEC.

Figure 7. - Flap noise radiation patterns. Microphone radius, 50 feet. Trailing flap angle, 60°.

E-7856

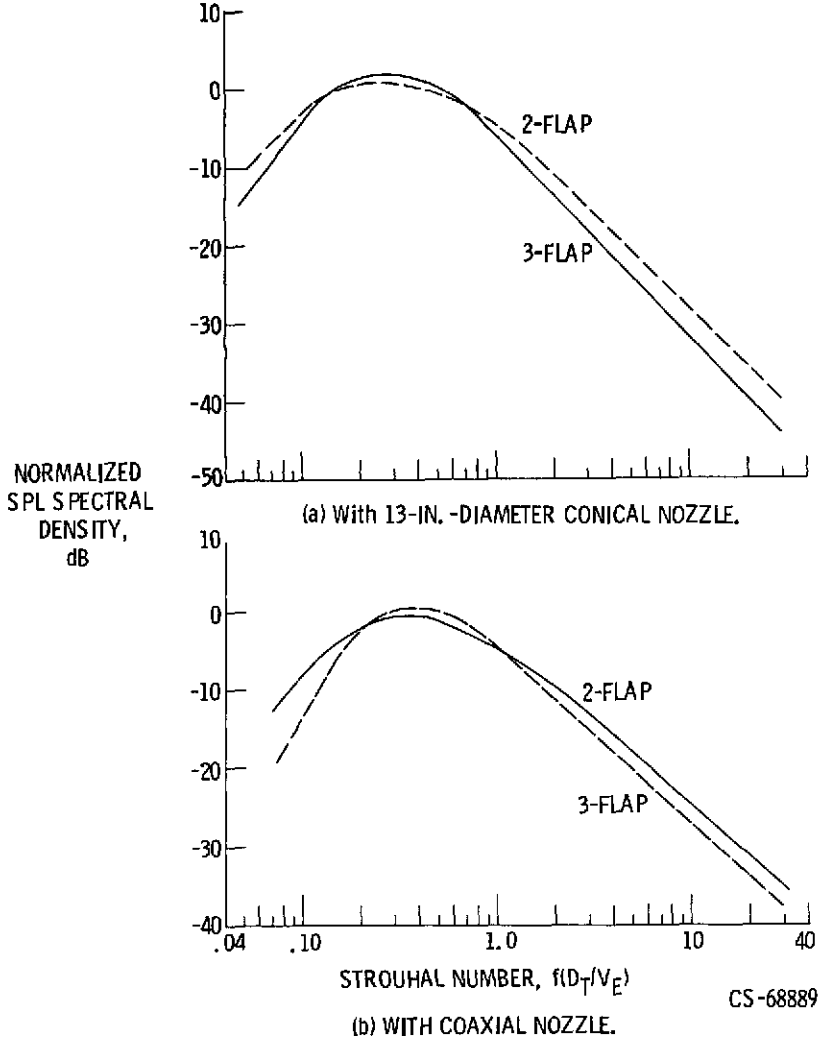


Figure 8. - Comparison of Strouhal correlations for baseline 2-flap and 3-flap configurations. Trailing flap angle, $60^0$; microphone angle, $70^0$.

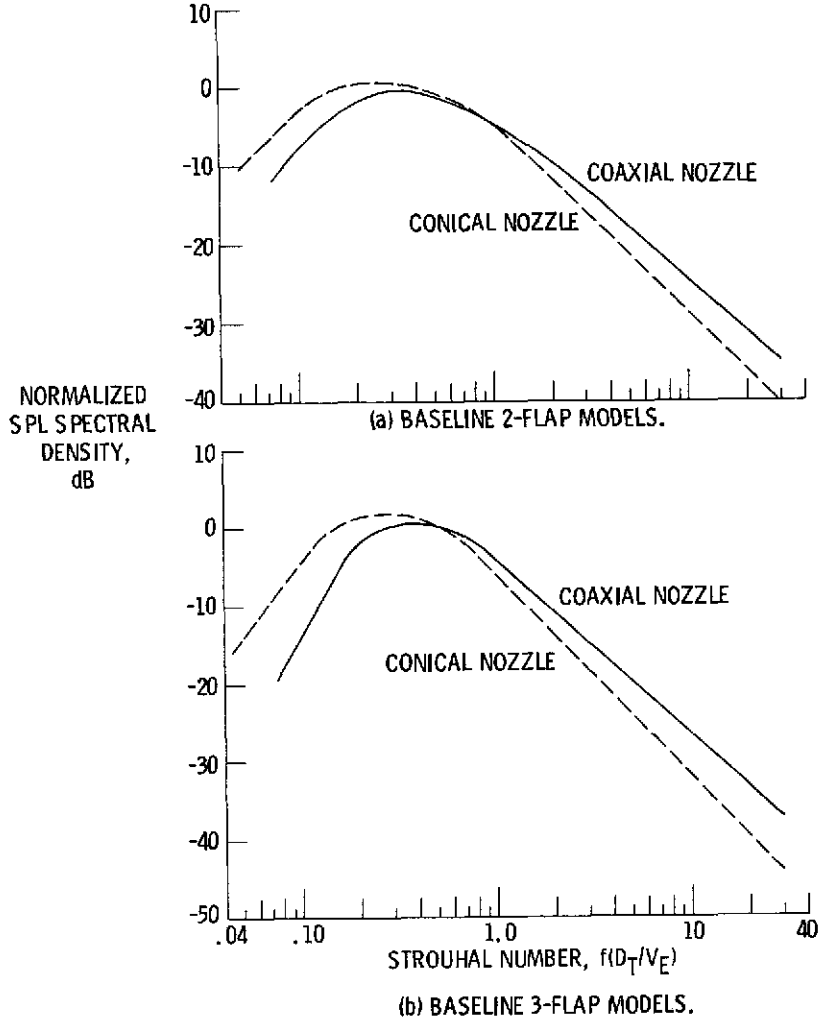


Figure 9. - Comparison of Strouhal correlations for 13-in. -diam. conical and coaxial nozzle configurations. Trailing flap angle, $60^0$; microphone angle, $70^0$.

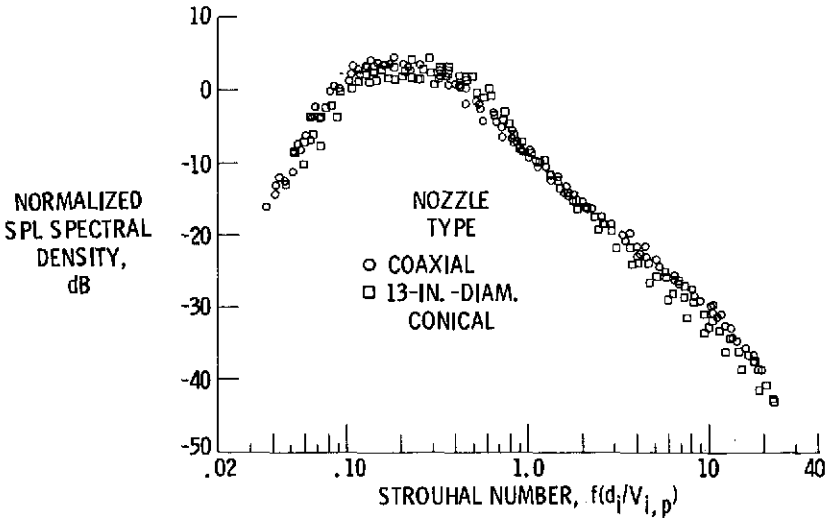


Figure 10. - Comparison of Strouhal correlations for baseline 3-flap coaxial and conical nozzle configurations based on impingement parameters. Trailing flap angle, 60°; microphone angle, 70°.



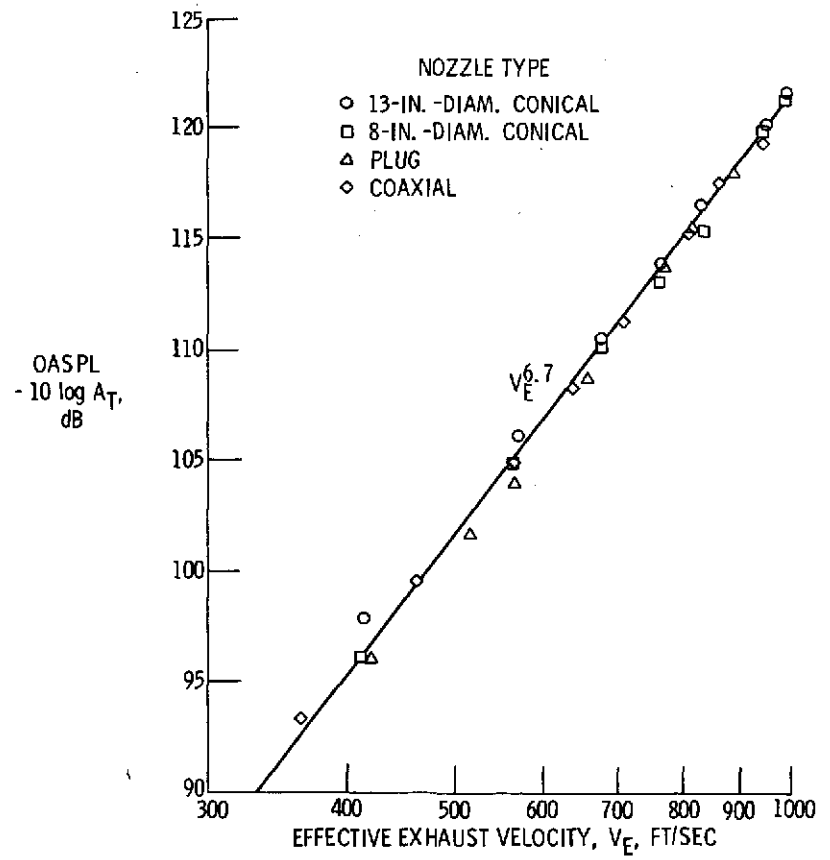


Figure 11. - Variation of normalized overall sound pressure level with nozzle exhaust velocity for 2-flap EBF configurations. Trailing flap angle, 60°; microphone distance, 50 ft; microphone angle, 70°; nozzle position, Y, 19.25 in.

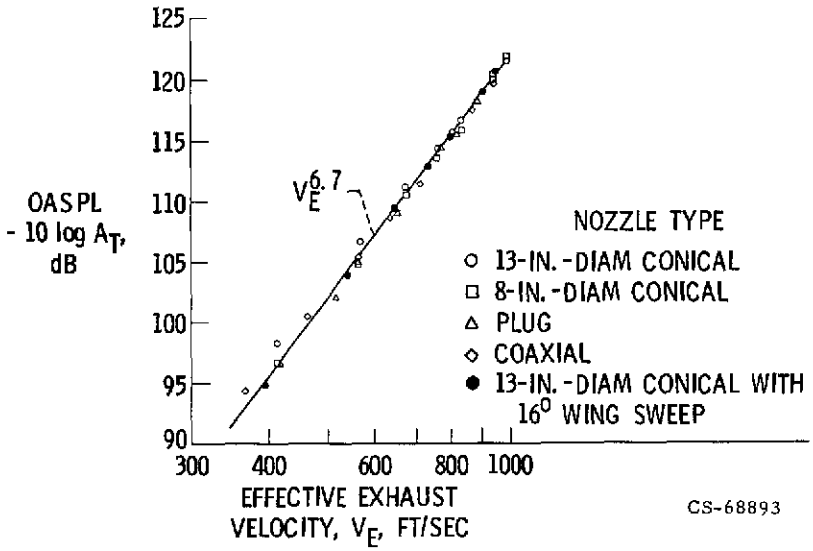


Figure 12. - Variation of normalized overall sound pressure level at radial peak angle with nozzle exhaust velocity for 2-flap EBF configurations. Trailing flap angle, 60°; microphone distance, 50 ft; nozzle position, Y, 19.25 in.

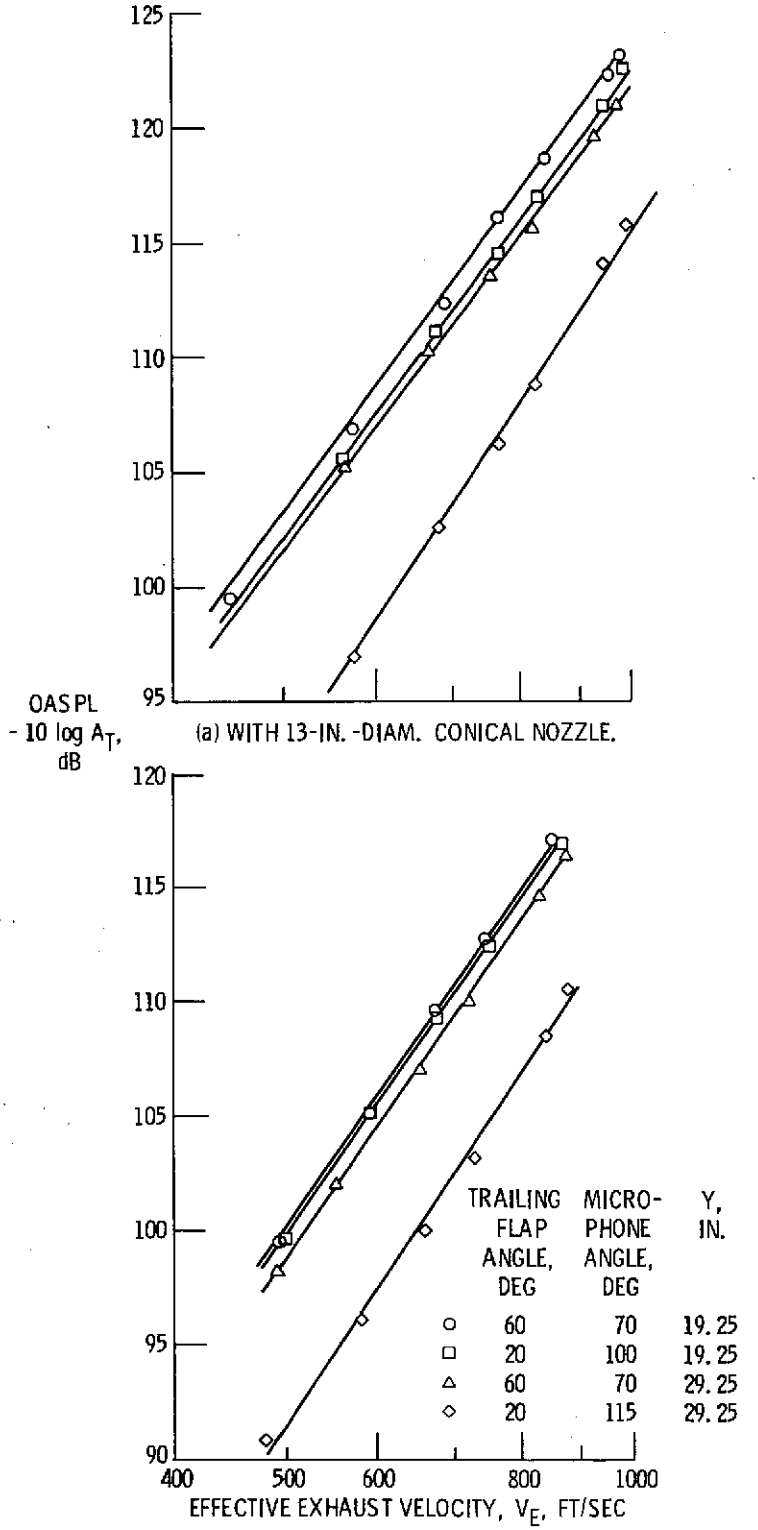


Figure 13. - Comparison of normalized OASPL for baseline and low-nozzle-position 3-flap configurations. Microphone angle corresponds to flyover maximum.

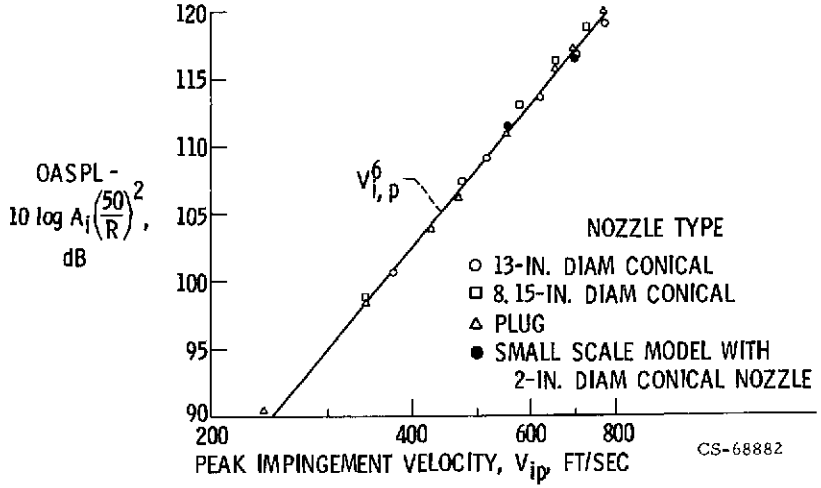


Figure 14. - Variation of normalized overall sound pressure level at radial peak angle with impingement velocity for 2-flap EBF configurations. Trailing flap angle, $60^0$; microphone distance, 50 ft.

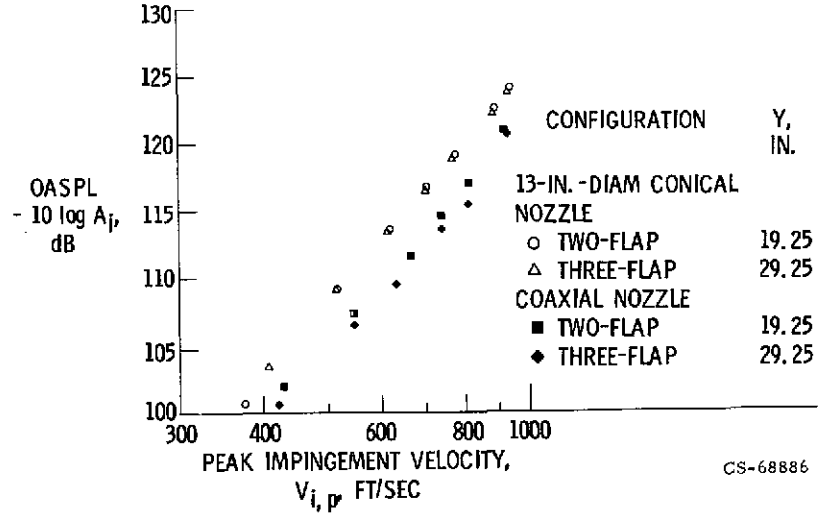


Figure 15. - Comparison of normalized OASPL at radial peak angle for coaxial and conical nozzle configurations. Trailing flap angle, $60^0$; microphone distance, 50 ft.



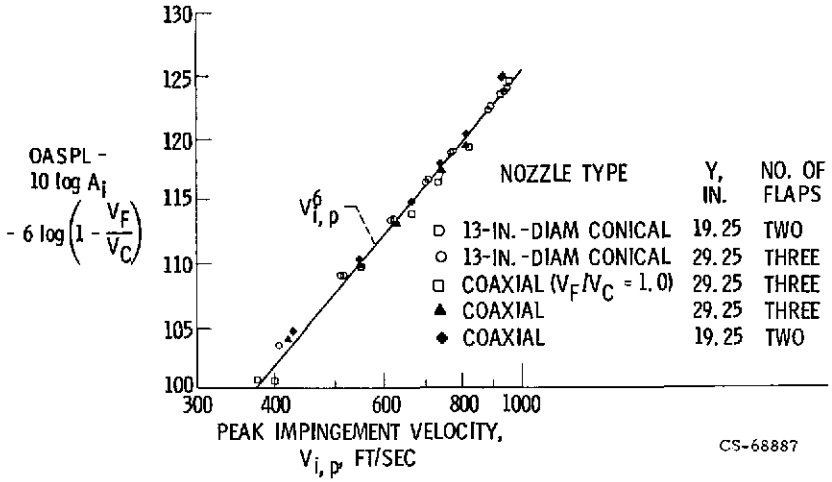


Figure 16. - Correlation of normalized OASPL at radial peak angle for coaxial and conical nozzle EBF configurations by including turbulent intensity parameter. Trailing flap angle, $60^0$; microphone distance, 50 ft.

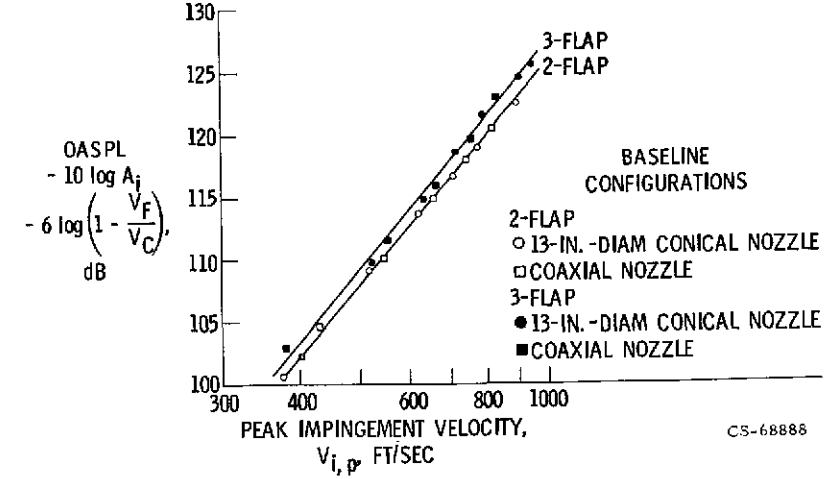


Figure 17. - Effect of number of flaps on normalized OASPL at radial peak angle for baseline configurations. Trailing flap angle, $60^0$; microphone distance, 50 ft.

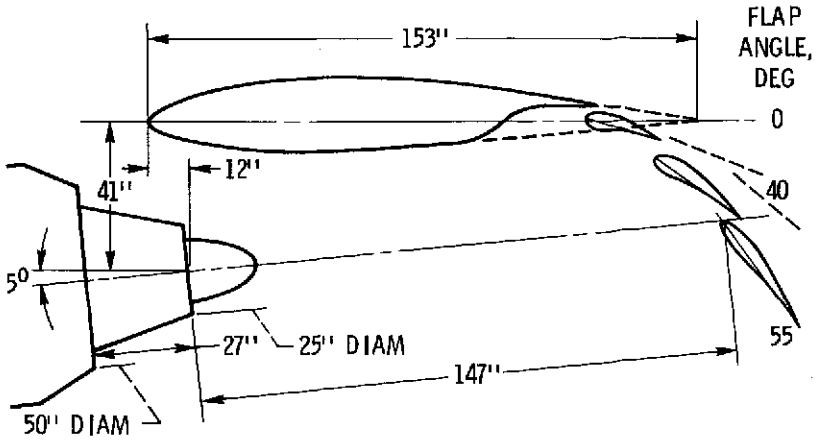


Figure 18. - Sketch of baseline turbofan engine under-the-wing test configuration. Core exhaust area, 1.94 sq ft; fan exhaust area, 5.49 sq ft.



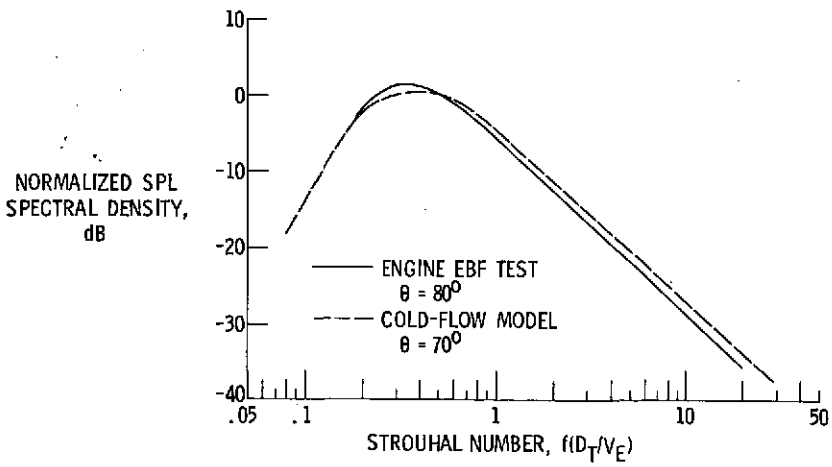


Figure 19. - Comparison of Strouhal correlations of noise spectra for baseline turbofan engine and cold-flow-model 3-flap EBF configurations. Trailing flap angle, 55° for engine test and 60° for model.

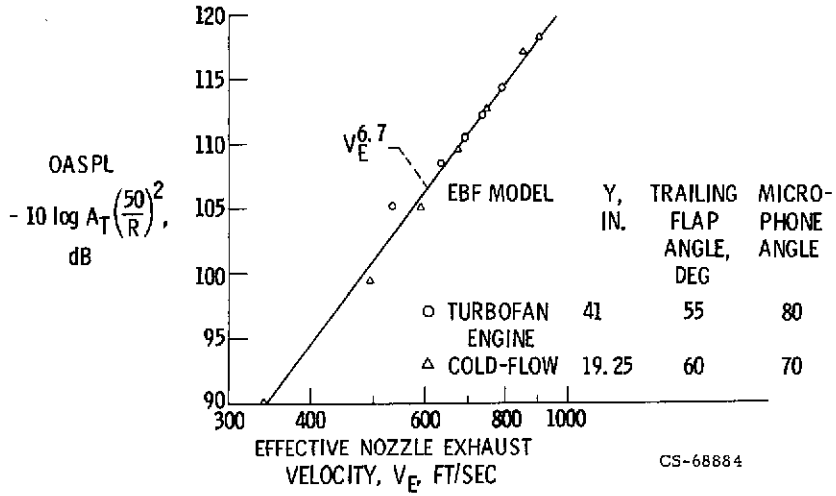


(a) CORRELATION BASED ON NOZZLE EXIT PARAMETERS.

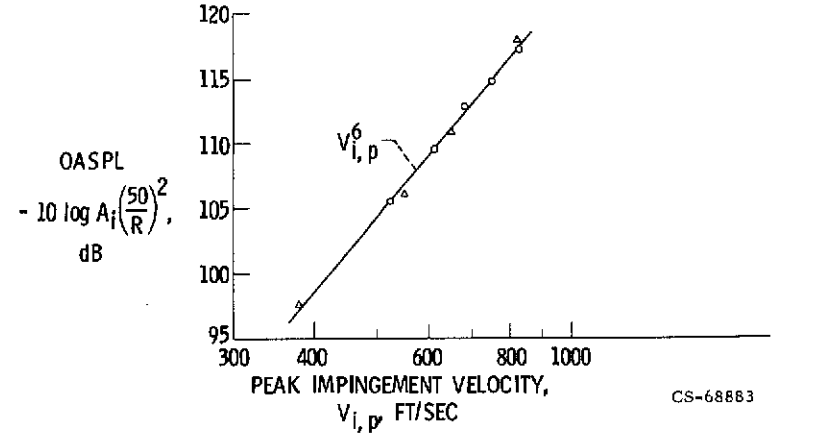


(b) CORRELATION BASED ON IMPINGEMENT PARAMETERS.

Figure 20. - Comparison of normalized OASPL for baseline turbofan engine and cold-flow 3-flap EBF configurations with approach flap position.

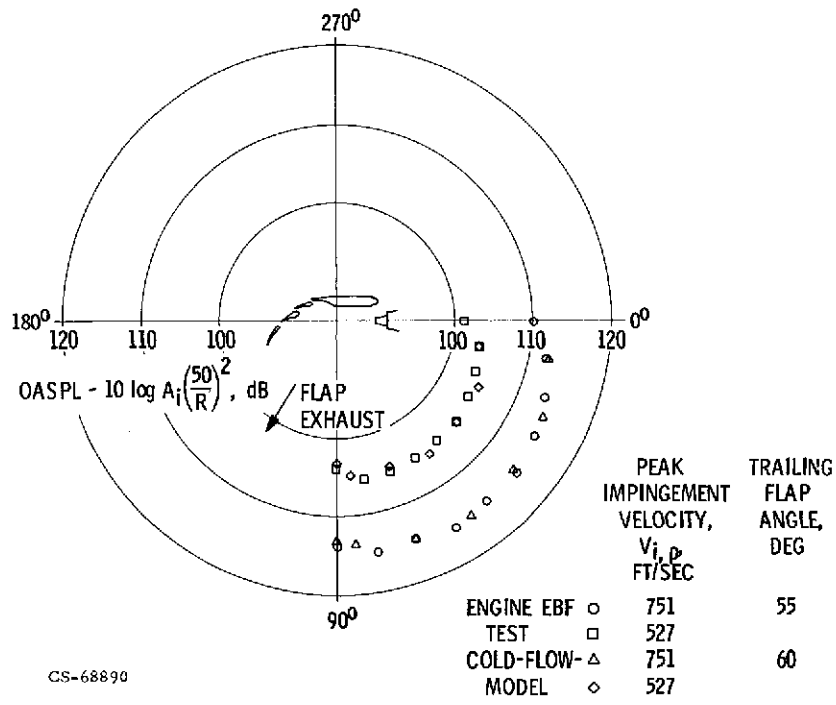


Figure 21. - Comparison of dipole flap-noise radiation patterns for turbofan engine and cold flow model externally blown flap systems at constant peak impingement velocity.



NASA-Lewis